


Article

# Gallium-Promoted Ni Catalyst Supported on MCM-41 for Dry Reforming of Methane

Ahmed S. Al-Fatesh <sup>1,\*</sup> , Ahmed A. Ibrahim <sup>1</sup>, Jehad K. Abu-Dahrieh <sup>2,\*</sup>,  
Abdulrahman S. Al-Awadi <sup>1</sup>, Ahmed Mohamed El-Toni <sup>3</sup>, Anis H. Fakeeha <sup>1</sup>  
and Ahmed E. Abasaed <sup>1</sup> 

<sup>1</sup> Chemical Engineering Department, College of Engineering, King Saud University, P.O. Box 800, Riyadh 11421, Saudi Arabia; aidid@ksu.edu.sa (A.A.I.); alawadi@ksu.edu.sa (A.S.A.-A.); anishf@ksu.edu.sa (A.H.F.); abasaed@ksu.edu.sa (A.E.A.)

<sup>2</sup> School of Chemistry and Chemical Engineering, Queen's University Belfast, Belfast BT9 5AG, Northern Ireland, UK

<sup>3</sup> King Abdullah Institute for Nanotechnology, King Saud University, Riyadh 11451, Saudi Arabia; aamohammad@ksu.edu.sa

\* Correspondence: aalfatesh@ksu.edu.sa (A.S.A.-F.); j.abudahrieh@qub.ac.uk (J.K.A.-D.); Tel.: +966-11-4676859 (A.S.A.-F.)

Received: 4 April 2018; Accepted: 23 May 2018; Published: 01 June 2018

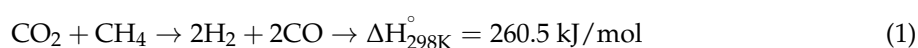


**Abstract:** The stability and catalytic activity of mesoporous Ni/MCM-41 promoted with a Ga loading of (0.0, 1.0, 1.5, 2.0, 2.5, and 3.0 wt %) as an innovative catalyst was examined for syngas production via CO<sub>2</sub> reforming of CH<sub>4</sub>. The objective of present work was to develop a potential catalyst for CO<sub>2</sub> reforming of methane. For this purpose different loadings of gallium were used to promote 5% nickel catalyst supported on MCM-41. An incipient wetness impregnation method was used for preparing the catalysts and investigated at 800 °C. Physicochemical characterization techniques—including BET, XRD, TPD, TPR, TEM, and TGA—were used to characterize the catalysts. The addition of small amounts of Ga resulted in higher surface areas with a maximum surface area of 1036 m<sup>2</sup>/g for 2.5% Ga. The incorporation of Ga to the catalyst decreased the medium and strong basic sites and reduced the amount of carbon deposited. There was no weight loss for 3%Ga+5%Ni/MCM-41. The 2% Ga loading showed the highest CH<sub>4</sub> conversion of 88.2% and optimum stability, with an activity loss of only 1.58%. The Ga promoter raised the H<sub>2</sub>/CO ratio from 0.9 to unity.

**Keywords:** CO<sub>2</sub> reforming; Ga promoter; mesoporous silica; stability

## 1. Introduction

Carbon dioxide is a greenhouse gas that contributes to more than 90% of the global greenhouse gas emissions. Increased greenhouse gas emissions increase global temperatures and change wind patterns [1]. Decreasing the amount of CO<sub>2</sub> in the atmosphere is the biggest challenge that needs new ideas and technologies. Chemical transformation of CO<sub>2</sub> into useful products is gaining attention. The high abundance and low cost of CO<sub>2</sub> are the main advantages of using it as a feedstock in organic syntheses [2,3]. Amongst the chemical transformation methods, dry reforming of methane (DRM), where methane and CO<sub>2</sub> are used as the feedstock to produce synthesis gas, is a very promising technology for environmental protection and energy production [2]. It produces H<sub>2</sub>/CO, which is one of the main building blocks of chemical and petrochemical products, in a ratio of unity.



Reaction in Equation (1) transforms  $\text{CH}_4$  and  $\text{CO}_2$  greenhouse gases into valuable syngas ( $\text{H}_2$  and  $\text{CO}$ ). The  $\text{CO}_2$ -reforming of  $\text{CH}_4$  has been examined with noble metals (Pt and Pd); although these metals showed considerable activity and stability, their high price and inadequate availability restrict their use. Transition metals such as Ni-based catalysts are cost-effective and exhibit similar activity to noble metals for (DRM) [4]. However, the disadvantage of Ni-based catalysts for DRM comes from the severe deactivation resulting from carbon deposition and loss of the active metal surface area by sintering [5–7]. Extensive research has been performed to design Ni-based catalysts that resist coking. The type of support for Ni-based catalysts shows an important role in the catalytic activity and distribution of the active metal sites [8]. There has been extensive research using different catalyst supports such as  $\text{CeO}_2$ - $\text{ZrO}_2$  [9,10],  $\text{Al}_2\text{O}_3$ - $\text{ZrO}_2$  [11], and  $\text{Al}_2\text{O}_3$ - $\text{MgO}$  [12].

Silicate-structured mesoporous materials like MCM-41 and SBA-15 have played a significant role as supports in catalysis research [13,14]. Chen et al. [15], showed the advantages of mesoporous silica supported on a Ni- $\text{La}_2\text{O}_3$  catalyst. The catalyst revealed good activity, stability, and efficiency for DRM. Excellent catalytic performance using MCM-41 support for the steam reforming of methanol has been reported in the literature [16,17]. Similarly, catalysts supported on MCM-41 displayed an excellent activity and stability in the DRM [18–21]. Ni particle dispersion into the structure of the porous support is another way to suppress carbon accumulation. Xu et al. [22] designed a mesoporous alumina supported catalyst that accommodated the dispersion of Ni. They reduced the coke formation by adding basic promoters into the structure of the alumina. Ordered mesoporous silica is appropriate for accommodating the nanoparticles of metals in its mesoporous structure. Specifically, the high surface areas of SBA-15 and MCM-41 promote the dispersion of Ni. The fixed Ni particles in the silica framework were stabilized by the channels in the silica framework [23]. The enhanced stability of Ni-based catalysts on mesoporous silica supports has been reported in DRM [4,19,20].

Further, a broad research has been carried out to alter the catalyst supports via promoters to slow the deactivation of Ni-based catalysts [24–26]. It was found that Rh added to the Ni/MCM-41 catalyst by the one-pot procedure improved both the activity and time-on-stream stability of the catalyst [24]. An optimum amount of gallium oxide was required to avoid extreme acidity and enhance butadiene selectivity when magnesium silicate catalysts promoted with Ga were used for the conversion of ethanol into butadiene [27]. The promotion with Ga of a  $\text{SiO}_2$ -supported Cu catalyst in the hydrogenation of  $\text{CO}_2$  to methanol was studied [28]. The results indicate that Ga promotes Cu and increases methanol selectivity, probably by forming new active sites during the methanol formation without altering the Cu oxidation state which, under reaction conditions, stays mostly metallic.

Ga is known to modify the acidic properties of the catalyst [27,29,30], while low Ga additions also increase the surface area [27]. The objective of present work was to develop a potential catalyst for  $\text{CO}_2$  reforming of methane. For this purpose, different loadings of gallium were used to promote 5% nickel catalyst supported on MCM-41. To our knowledge, there is no reported work on using Ga as a promoter for DRM. This study will explore Ga as a promoter in Ni/MCM-41 catalysts and investigate the effect of different loadings (0.0, 1.0, 1.5, 2.0, 2.5, and 3.0 wt %) of Ga on Ni/MCM-41. The catalysts were tested using TPD, BET, XRD, TPR, TEM, and TGA.

## 2. Results and Discussion

Figure 1, depicts the  $\text{N}_2$  adsorption-desorption isotherms of 5%Ni+x%Ga/MCM-41 ( $x = 0, 1, 1.5, 2, 2.5$ ) catalysts, while Table 1 presents the pore diameter, surface area, and pore volume for the modified and unmodified Ni-based catalysts. The modification by small amounts of Ga resulted in higher surface areas with a maximum surface area of  $1036 \text{ m}^2/\text{g}$  for 2.5% Ga; conversely, as the loading increased to 3%, the surface area slightly decreased. A plausible explanation for the effect of the promoter Ga relates to the fact that small amounts Ga increases the dispersion of the active metals of the catalyst. However, when the amount is further increased, it is possible that it overlaps the Ni sites promoting multilayer deposition—hence reducing the available surface area. This factor was observed before [31]. The MCM-41 was prepared from different precursors and verified the tested one

in this work and the surface area determination was repeated. The result was placed in the revised manuscript. The BET value for bare MCM-41 tends to be 1132.72 m<sup>2</sup>/g.

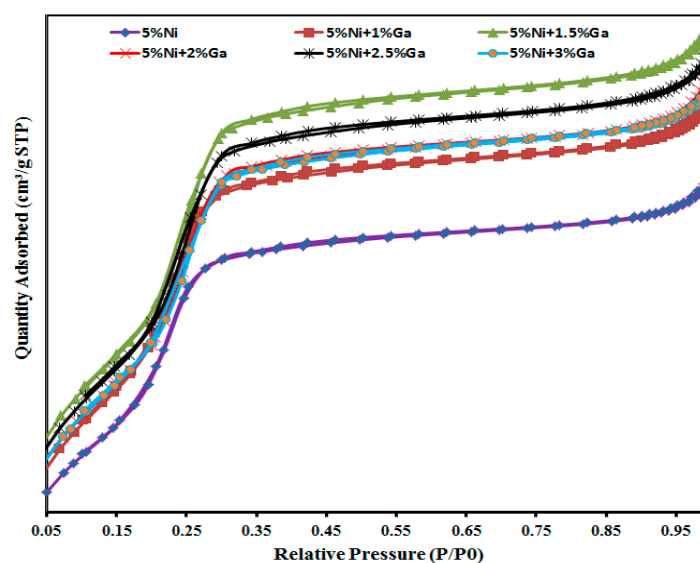


**Figure 1.** N<sub>2</sub> adsorption–desorption isotherms of fresh tested catalysts.

**Table 1.** Characterization of the catalysts used for methane reforming

Catalyst	BET m <sup>2</sup> g <sup>-1</sup>	P.V cm <sup>3</sup> g <sup>-1</sup>	P.D nm
MCM-41	1132.72	0.664	2.57
5%Ni/MCM-41	897.85	0.485	2.48
1%Ga+5%Ni/MCM-41	917.38	0.664	2.74
1.5%Ga+5%Ni/MCM-41	978.56	0.660	2.74
2%Ga+5%Ni/MCM-41	983.33	0.664	2.74
2.5%Ga+5%Ni/MCM-41	1036.02	0.593	2.57
3%Ga+5%Ni/MCM-41	979.91	0.560	2.57

BET Surface Area; P.V BJH Adsorption Cumulative Volume of Pores Between 1700 nm and 300nm diameter; P.D BJH Adsorption average pore diameter ( $4v/A$ ).

The variation of pore diameter, surface area, and the pore volume was not significant for the modified catalysts. As a consequence, there is no connection to be made between the catalytic activity and the surface area of the samples.

X-ray diffraction patterns for fresh and spent 5%Ni+x%Ga/MCM-41 ( $x = 0.0, 1.5, 2.0, 2.5,$  and  $3.0$ ) catalysts are shown in Figure 2. It can be observed that MCM-41 has no diffraction peaks due to the amorphous nature of mesoporous silica. Upon the XRD measurement for the fresh calcined Ni loaded sample (Figure 2a), NiO characteristic peaks were observed which is consistent with JCPDS no. 01-089-5881. The addition of various amounts of Ga did not lead to the appearance of any new phases, but only increased the intensity of the NiO peaks, suggesting that Ga enhanced the crystallization and growth of the Ni particles. However, after performing the H<sub>2</sub> reduction on the spent samples (Figure 2b), the X-ray diffraction patterns were significantly changed due to the formation of a Ni phase with its characteristic peak (111) at  $2\theta = 45^\circ$  and (200) peak at  $2\theta = 53^\circ$ . However, another strong diffraction peak, observed at  $2\theta = 28^\circ$ , could be attributed to crystallized silica because of the high temperature and reduction conditions. The peak at  $2\theta = 30^\circ$  could be attributed to the Ga metal formed from the reduction reaction. The main peaks at  $2\theta = 35, 45, 47, 50,$  and  $53^\circ$  could be due to the formation of Ni-Ga intermetallic compounds [32,33]. The amount of Ga loading, however, did not affect the Ni-Ga intermetallic phase.

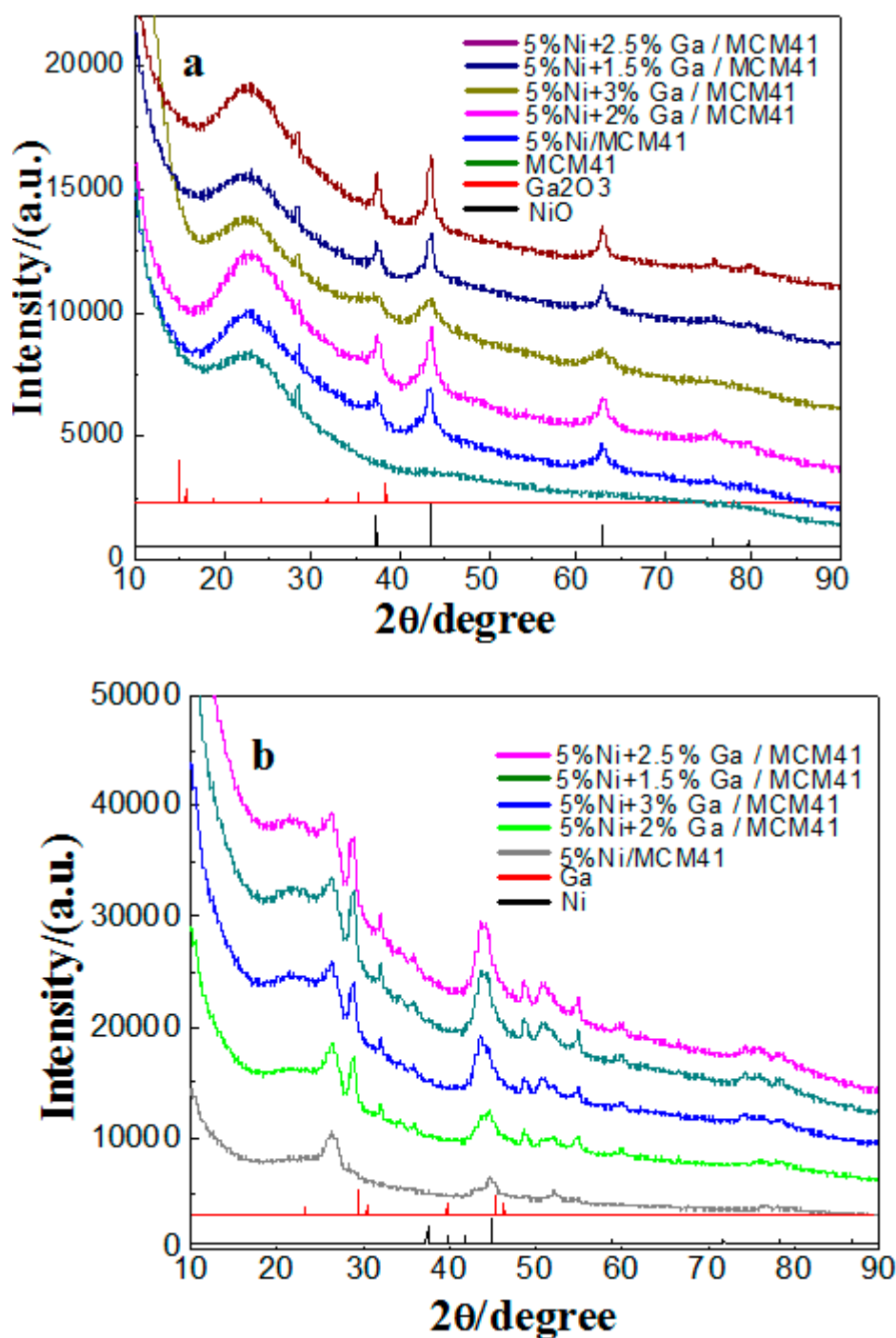


Figure 2. XRD patterns of (a) fresh and (b) used: 5%Ni+x%Ga/MCM-41 ( $x = 0, 1.5, 2.0, 2.5, 3.0$ ) catalysts.

Figure 3 shows the H<sub>2</sub>-TPR profiles of the 5%Ni/MCM-41, 1.0%Ga5%Ni/MCM-41, 1.5%Ga5%Ni/MCM-41, 2.0%Ga5%Ni/MCM-41, 2.5%Ga5%Ni/MCM-41, and 3.0%Ga5%Ni/MCM-41 samples. All catalysts showed two main reduction peaks except the 3.0%Ga5%Ni/MCM-41. It can be viewed that the intensity of the first peak decreased and slightly shifted as the Ga loading increased and eventually disappeared for the 3.0% Ga loading. Both 2.5% Ga and 3.0% Ga presented peaks at high temperatures indicating the relatively stronger metal support interactions compared to other % loadings of Ga. It can also be seen that there was no reduction peak before 360 °C for all catalysts; this implies the disappearance of NiO on the silica pore wall surface [20]. The second peak was significantly shifted from 520 °C to 700 °C for 0.0% and 3.0% Ga, respectively, and the peak intensity

broadened. This can be interpreted as the reduction of Ni ions situated at different layers in the pore wall [20], indicating an intense interaction between the Ni particles and the MCM-41 support. The shift of TPR peaks might be reasonably attributed to the strong interaction between the metal and the support and by a reduction in the particle size of the bulk material to ultrafine particles [34].

Owing to the introduction of the second metal, some variations in the reduction configurations are expected for the bimetallic MCM-41 catalysts [4]. The major peak is tentatively attributed to the reduction of  $\text{Ni}^{2+}$  in the silica structure, although the reduction of the small amount of doped Ga species cannot be excluded [4]. It is clear that the amount of incorporated Ga had a significant influence on the reducibility of the catalysts. It is known that a stronger interaction between the metal and support requires a higher temperature for hydrogen reduction [35].

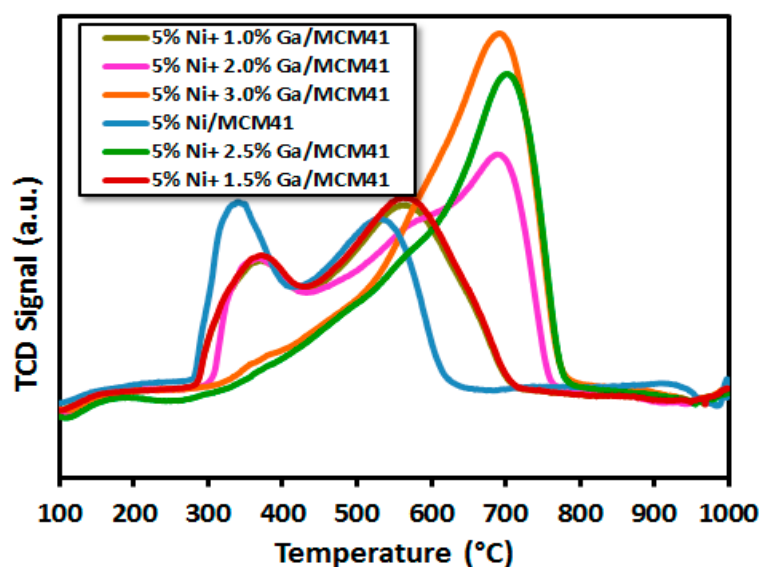


Figure 3. TPR patterns for promoted and non-promoted 5% Ni/MCM-41 catalysts.

$\text{CO}_2$ -TPD was used to measure the basic sites existing in the catalysts. The temperature programmed desorption technique permits the determination of the strength of acidic/basic sites present on the catalyst surface, together with total basicity. Usually in TPD the strengths of the basic sites are reported in terms of temperature range where the chemisorbed  $\text{CO}_2$  on the basic sites is desorbed; adsorbate on weaker sites desorbs at lower temperature and that adsorbed on stronger sites desorbs at higher temperature. A low desorption temperature represents  $\text{CO}_2$  adsorption on weak basic sites, whereas a high desorption temperature represents strong basic sites [22]. The  $\text{CO}_2$ -TPD for 5%Ni/MCM-41, 1%Ga5%Ni/MCM-41, and 2%Ga5%Ni/MCM-41 catalysts are compared in Figure 4. All catalysts showed identical  $\text{CO}_2$ -TPD profiles with three desorption peaks. As shown in Table 2 and Figure 4, each desorption temperature reflects the strength of the basic sites, whereas the area under the curve of each peak represents the amount of desorbed  $\text{CO}_2$  that correlates with the number of basic sites [36]. For example, the desorption peaks for 5%Ni/MCM-41 catalyst centered at 78, 271, and 678 °C had a total basic amount of  $234.45 \mu\text{mol g}^{-1}$ , as listed in Table 2. It can be seen that with the incorporation of Ga into the Ni/MCM-41 catalyst, the desorption peaks shifted to higher temperatures. However, while the intensity of weak basic sites increased, the intensity of the strong and medium basic sites decreased. The decrease in the number of medium and strong basic sites could be ascribed to the formation of extra-framework acid sites [30]. There was a remarkable decrease in the total basic site density as the Ga loading increased e.g., from  $234.45$  to  $142.69 \mu\text{mol g}^{-1}$  for 5%Ni/MCM-41 and 2%Ga5%Ni/MCM-41 catalysts, respectively.

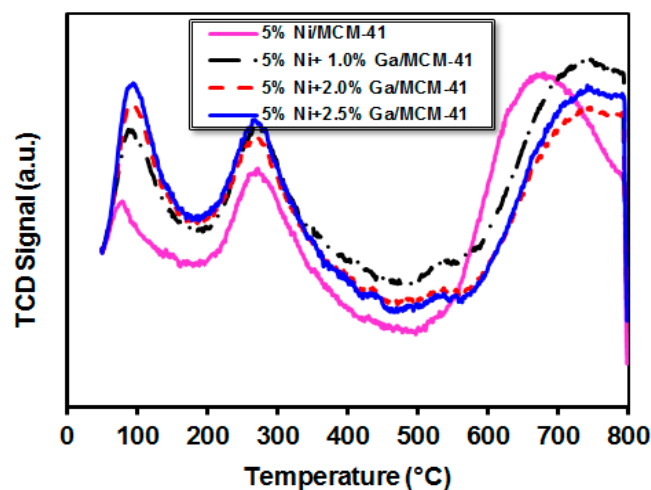


Figure 4. CO<sub>2</sub>-TPD profiles of 5%Ni+x%Ga/MCM-41. (x = 1.0, 2.0, 2.5).

Table 2. Amount of CO<sub>2</sub> desorbed with respect to the peaks.

Catalyst	50–170 °C μmol g <sup>-1</sup>	170–500 °C μmol g <sup>-1</sup>	500–800 °C μmol g <sup>-1</sup>	Total μmol g <sup>-1</sup>
5%Ni/MCM-41	8.79	43.32	182.35	234.45
1.0%Ga5%Ni/MCM-41	20.26	33.87	110.60	164.73
2.0%Ga5%Ni/MCM-41	22.74	26.30	93.65	142.69
2.5%Ga5%Ni/MCM-41	23.15	42.90	79.13	145.18

Thermogravimetric analyses (TGA) of both fresh and spent catalysts were used to quantitatively measure the carbon formation during the reaction. The TGA analysis was carried out under air atmosphere. The life of the spent catalyst was about a day. For the fresh catalyst, the TGA analysis showed no weight loss and hence no carbon deposition. The typical TGA results from spent catalysts are shown in Figure 5. A significant weight loss was observed between 600 and 750 °C. This can be explained by the combustion of the carbon deposited on the catalyst [24]. Increasing the Ga content in the catalyst decreased the amount of carbon. For example, for 5% Ni/MCM-41, the weight loss was about 16%; however, there was no weight loss for 3.0%Ga5%Ni/MCM-41. This change in weight loss cannot be correlated to the catalytic activity. It is possible that the deactivation of this catalyst is not due to carbon deposition on the external surface, but perhaps due to the deposition of carbon within the pores of the MCM-41 support which would be an irreversible deactivation. It could also be due to the destruction of the MCM-41 structure due to high Ga content.

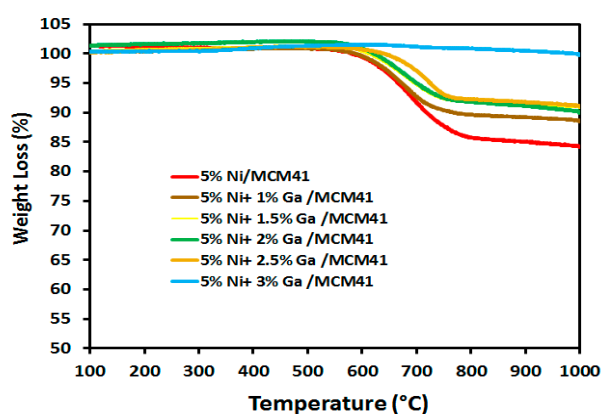
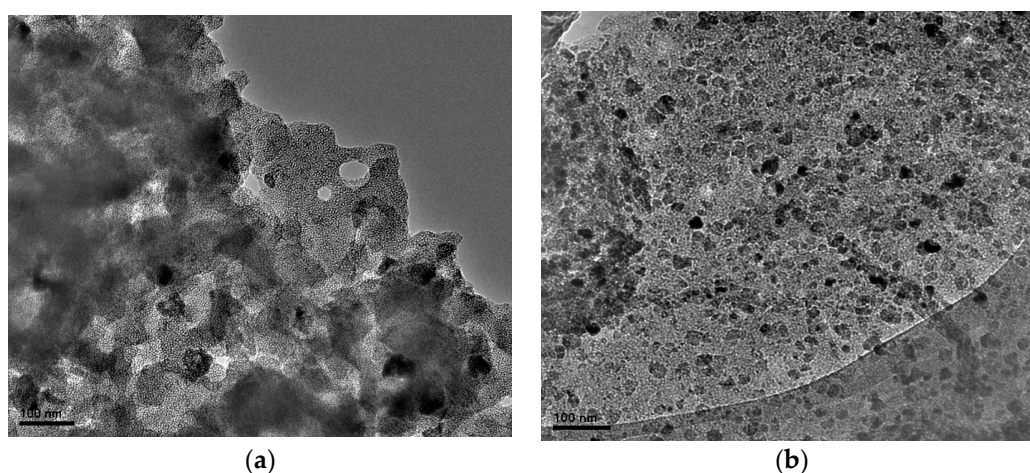


Figure 5. TGA curves for the used catalysts under atmospheric pressure with a heating rate of 20 °C/min.

Figure 6a,b display the TEM images of the 5%Ni/MCM-41 and 2%Ga5%Ni/MCM-41, respectively. The images show that the uniform ordered hexagonal pores of MCM-41 are still observed after metal loading [17], i.e., the long ordered arrangement of the channels in the matrix are preserved [37]. This demonstrates that the Ni particles were homogeneously dispersed in the form of round nanoparticles. The TEM images presented in Figure 6 reveal an average particle size that ranges from 25–40 nm for 5%Ni/MCM-41 and 16–33 nm for 2%Ga5%Ni/MCM-41. The uniform distribution of the Ni nanoparticles in the MCM-41 framework is apparent from the TEM image in Figure 6b.



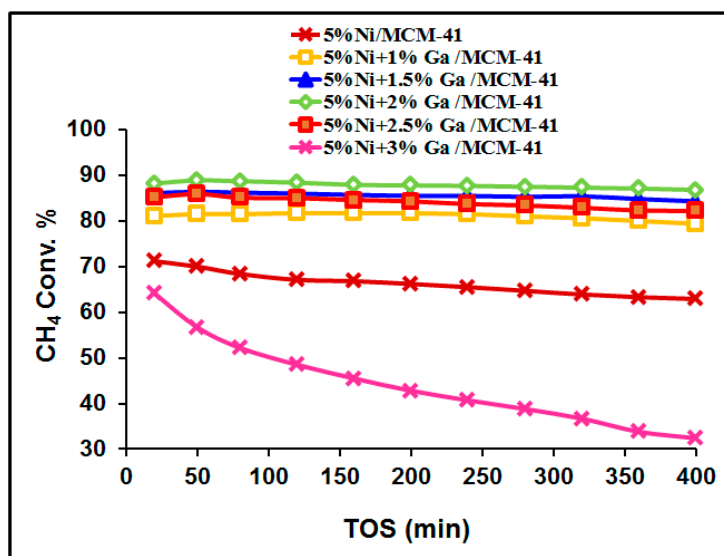
**Figure 6.** TEM analysis of the fresh catalyst, (a) 5%Ni/MCM-41 and (b) 2%Ga5%Ni/MCM-41.

The locations with darker contrast in the images in Figure 6a are ascribed to the Ni particles [36]. The minor dark spots are attributed to Ni particles located in the channels of the MCM-41 support. The larger dark areas over the pores correspond to Ni oxide agglomerates on the external surface, which resulted from the migration of Ni species out of the supports during the calcination process [34,37]. It can be seen that the Ni nanoparticles (dark points) were embedded within the mesoporous structure when Ga was introduced [38], which reduced the aggregation of NiO nanoparticles during the calcination step [39]. This observation further supports the bigger and larger reduction of the peak of Ga-Ni nanoparticles (TPR, Figure 2) in the chemisorption experiment. TEM images demonstrated a nearly regular hexagonal array of mesoporous channels of the catalyst [40]. The CH<sub>4</sub> and CO<sub>2</sub> conversions are presented in Figure 7. In this investigative stage, we have used TOS to reflect the stability of the Ga-promoted Ni/MCM-41. In this investigation we have not quantified the total number of active sites to determine the turn over frequency. As shown, both CH<sub>4</sub> and CO<sub>2</sub> conversions did not change for the catalysts with Ga loadings from 1–2.5% during the reaction period of 400 min. However, the 3% Ga loading showed lower activity and lesser stability than the 0% Ga-loaded catalyst. This is either because the catalyst is not easily reduced as shown in Figure 2, or due to the destruction of the framework of the MCM-41 support. Ga-incorporated Ni catalysts showed higher catalytic activity than that of the unmodified Ni-MCM-41 (0% Ga) catalyst, except for 3% Ga loading. This indicates that there should be an optimum Ga loading to enhance the catalytic activity and stability. As shown in Figure 8, 2% Ga loading showed a higher conversion of CH<sub>4</sub> and lower activity loss of 88.2% and 1.58%, respectively. The main disadvantage of using catalysts for this process is due to the deactivation. This phenomenon cannot be avoided, but often reduced to an acceptable level. For instance, 2% Ga loading catalyst (2%Ga5%Ni/MCM-41) showed a higher conversion of CH<sub>4</sub> (88.2%) and lower activity loss of 1.58%, for 400 min of TOS.

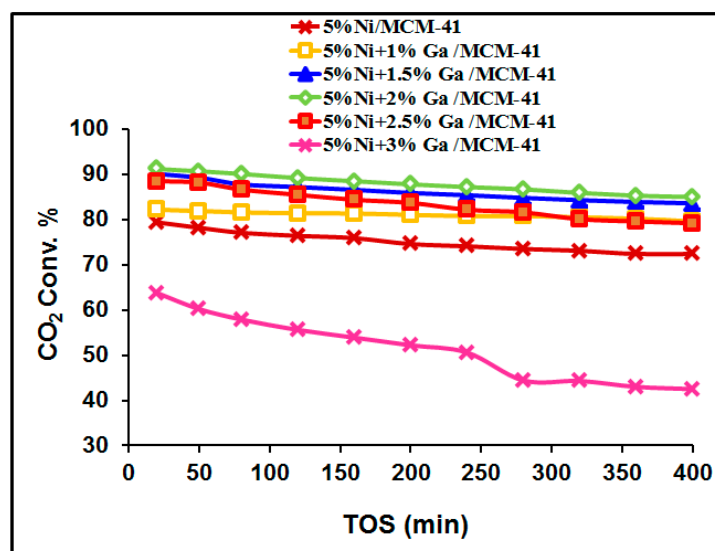
The most obvious disadvantage of Ni-based catalysts is the poor stability and a H<sub>2</sub>/CO ratio of less than unity, which is partly caused by the reverse water gas shift (RWGS) reaction. The H<sub>2</sub>/CO ratios for the different Ga loadings are shown in Figure 9. It is clear that the Ga promoter had a significant effect on the H<sub>2</sub>/CO ratio as the ratio increased from 0.9 to unity with the addition of Ga. This improvement could

possibly be related to the Ga-suppression of the RWGS reaction and/or the enhancement of the DRM rate ( $H_2$  formation rate) relative to the RWGS reaction [28].

Figure 10 shows the  $H_2/CO$  ratios and the conversions of  $CO_2$  and  $CH_4$  versus time-on-stream and  $H_2$  selectivity for the 2.0%Ga5%Ni/MCM-41 catalyst. The  $CH_4$  conversion profile indicates the stability and performance. The activity reduction was  $\sim 8\%$  during the 30 h time-on-stream. The carbon formation on the catalyst is the cause of the observed deactivation. Likewise, the  $CO_2$  profile presents a deactivation of approximately 5.3%. The conversions of  $CO_2$  are higher than the corresponding  $CH_4$  conversion since  $CO_2$  reacts with the produced  $H_2$  to form water and additional CO that lowers the ratio of  $H_2/CO$ . The generated  $H_2O$  in this step helped to remove the carbon deposits and hence contributed to the efficiency of the catalyst. Alternatively, the  $H_2/CO$  profile gave a near-unity value, indicating good stability for the 2.0%Ga5%Ni/MCM-41 catalyst. The  $H_2$  selectivity curve provided a steady and stable profile for all 30 h time on stream demonstrating the superiority of 2.0% Ga loading.



(a)



(b)

**Figure 7.** Graph of the (a)  $CO_2$  conversion and  $H_2/CO$  ratio and (b)  $CH_4$  conversion with time over different nickel based catalysts at reaction temperature of  $800\text{ }^\circ\text{C}$ , at atmospheric pressure,  $CH_4:CO_2 = 1:1$  in the feed gas, catalyst weight: 0.1 g, WHSV:  $21,000\text{ mL g}^{-1}\text{ h}^{-1}$ .



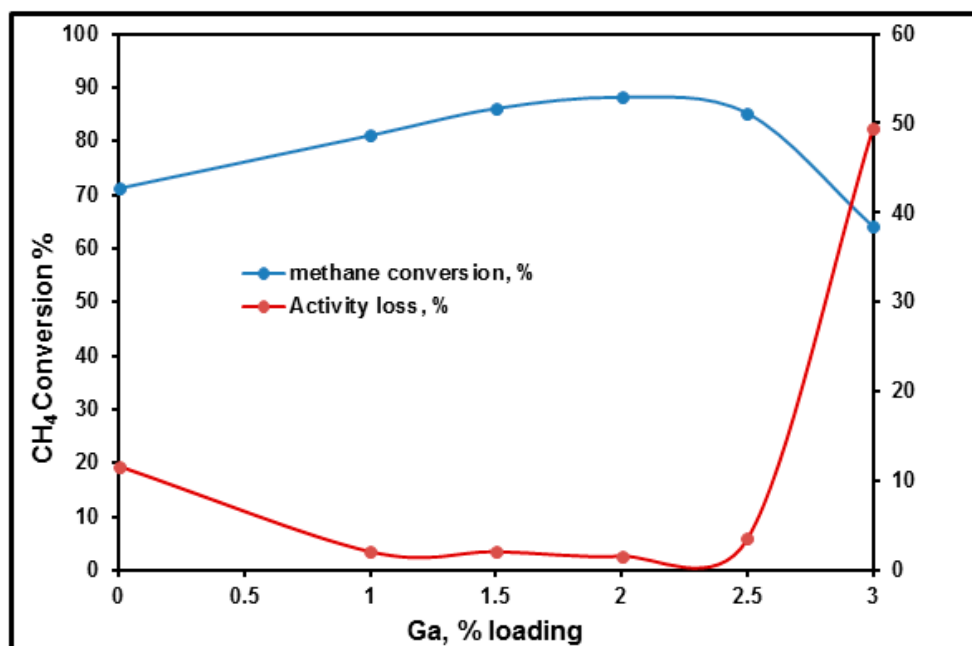


**Figure 8.** Effect of Ga loading on CH<sub>4</sub> conversion and deactivation over 400 min on stream at 800 °C reaction temperature, at atmospheric pressure, CH<sub>4</sub>:CO<sub>2</sub> = 1:1 in the feed gas, catalyst weight: 0.1 g, WHSV: 21,000 mL g<sup>-1</sup> h<sup>-1</sup>.

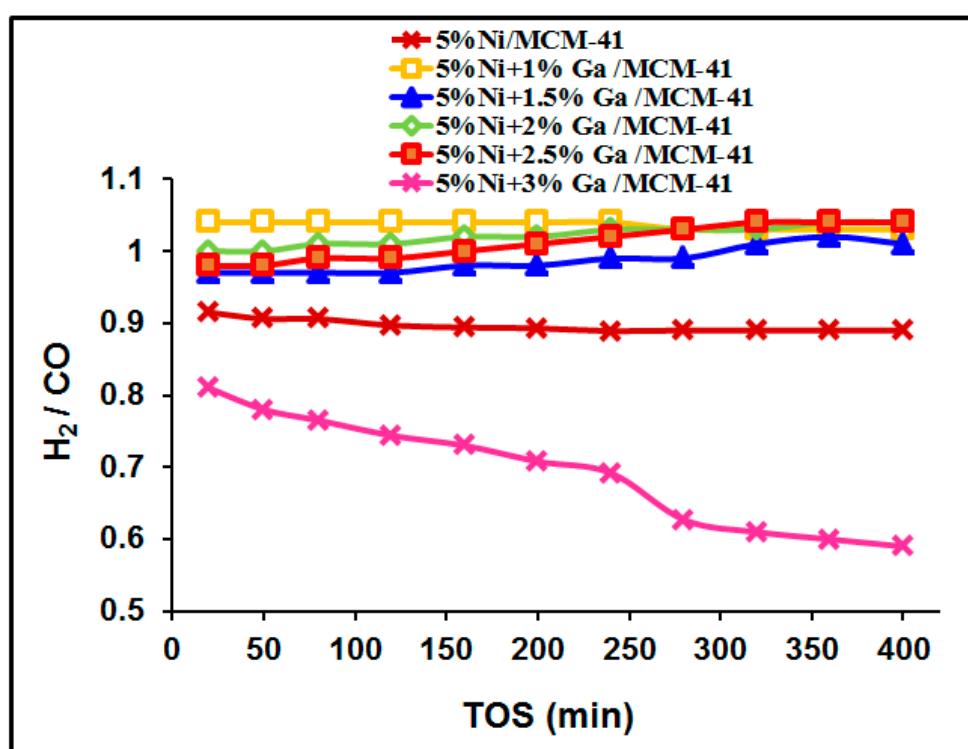


**Figure 9.** Graph of H<sub>2</sub>/CO ratio with time over different nickel-based catalysts at 800 °C reaction temperature, at atmospheric pressure, CH<sub>4</sub>:CO<sub>2</sub> = 1:1 in the feed gas, catalyst weight: 0.1 mg, WHSV: 2100 mL g<sup>-1</sup> h<sup>-1</sup>.

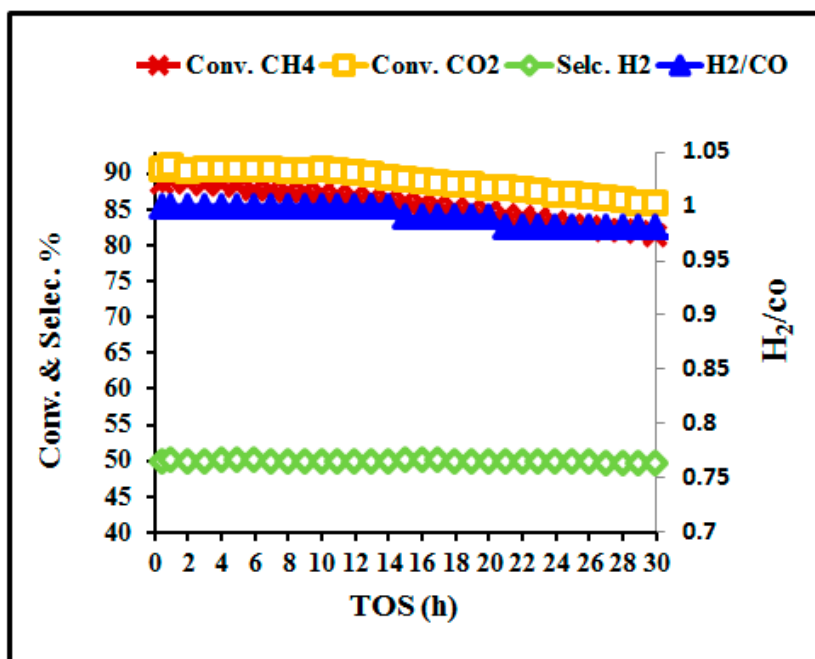


**Figure 10.** CH<sub>4</sub> & CO<sub>2</sub> conversions, H<sub>2</sub> selectivity & H<sub>2</sub>/CO ratio versus time on stream (TOS) for 5%Ni+2.0%Ga/MCM-41 catalyst at Tr = 800 °C; WHSV = 39,000 mL/min·gcat). Total flow rate = 40 mL/min (CH<sub>4</sub> = 30 mL/min, CO<sub>2</sub> = 30 mL/min & N<sub>2</sub> = 5 mL/min).

### 3. Materials and Methods

#### 3.1. Catalyst Preparation

MCM-41 was synthesized at room temperature (25 °C) using n-hexadecyltrimethylammonium chloride (HTMACl) as the template and tetraethyl orthosilicate (TEOS) as the silica precursor. In a typical synthesis, 392 mL of distilled water, 33 mL of ammonia (28–30% aqueous solution, Sigma-Aldrich, Saint Louis, MO, USA), and 34.05 mL of HTMACl (25% aqueous solution, Sigma-Aldrich) were mixed with vigorous stirring for 10 min, following which 36.45 mL of the silica source, TEOS (98%, Sigma-Aldrich) was added under stirring. Vigorous stirring was continued for 1 h at room temperature. After that, the resulting solid was filtrated and washed several times with distilled water. The washed solid was then dried at 80 °C overnight in a vacuum furnace. Subsequently, the synthesized material was heated up 600 °C to remove the surfactant [41].

Supported Ni catalysts were obtained by the incipient wetness impregnation method. The desired weight of [Ni(NO<sub>3</sub>)<sub>3</sub>·6H<sub>2</sub>O] was placed in double-distilled water, following which the MCM-41 support was impregnated with the active metal salt. The active metal impregnation of the support was performed under stirring at 80 °C for 3 h. then the impregnated catalysts were dried at 120 °C for 12 h, followed by 3 h calcination at 600 °C. The prepared catalysts were then reduced at 800 °C for 1 h under H<sub>2</sub>/Ar flow mixture (20/80). The conventional method of catalyst reduction at temperatures below and equal to calcination temperatures is not anymore maintained, partly because it has been observed in TPR that some peaks appear at temperatures higher than that of calcination temperature. Han et al. calcined their catalyst at 550 °C and performed the reduction and reaction at 800 °C [41]. The Ni amount was fixed at 5 wt %; in a previous publication, the optimum amount of Ni was about 5% [42]. The 5 wt % Ni/MCM-41-promoted catalysts with various loadings of Ga (0.0, 1.0, 1.5, 2.0, 2.5, and 3.0 wt %) were formed from the co-impregnation of Ni (NO<sub>3</sub>)<sub>3</sub>·6H<sub>2</sub>O and Ga(NO<sub>3</sub>)<sub>3</sub>·H<sub>2</sub>O using an MCM-41 support as described above. An elemental analysis of fresh 5%Ni+2.0%Ga/MCM-41 catalyst was performed to verify the desired composition. Figure 11 and the embedded table display the spectrum and the elemental compositions from qualitative and quantitative points of view. The embedded table denotes

the masses of the catalyst containing about 5% Ni and 2% Ga. Thus the EDX result confirmed that the desired catalyst was achieved.

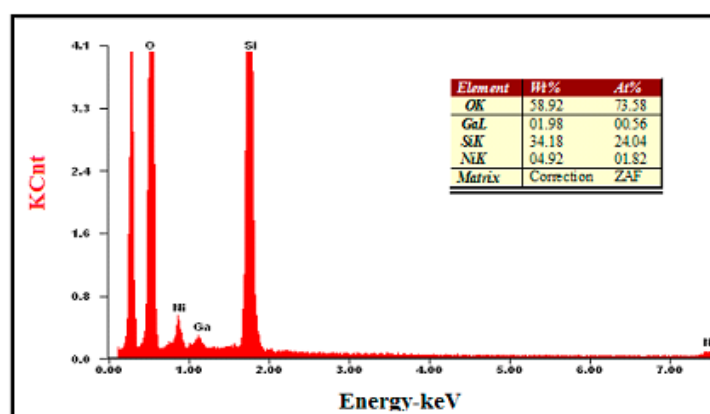


Figure 11. EDX diagram of fresh 5%Ni+2%Ga/MCM-41 catalyst.

### 3.2. Catalytic Activity Test

DRM was carried out at 1 bar in a tubular micro-reactor (ID = 9 mm). The setup of Figure 12 was supplied by PID Eng. and Tech. Prior to the DRM reaction, 0.10 g sample was activated in situ under  $H_2$  flow (20 mL/min) at 800 °C for 60 min. The reactor was then flushed with  $N_2$  for 20 min. The catalyst was then kept at the reaction temperature (800 °C) under  $N_2$  flow, while the reactants  $CH_4$ ,  $CO_2$ , and  $N_2$  were simultaneously introduced at flow rates of 30, 30, and 5 mL/min respectively. The temperature, pressure, and reaction variables were monitored through the reactor panel and a GC (GC-2014 SHIMADZU) unit. Duplicate runs were performed; the variation was within  $\pm 5\%$ . The conversions of the reactants were determined using the following equations, respectively.

$$\%CH_4 \text{ conversion} = \frac{CH_4 \text{ (in)} - CH_4 \text{ (out)}}{CH_4 \text{ i}} \times 100 \quad (2)$$

$$\%CO_2 \text{ conversion} = \frac{CO_2 \text{ (in)} - CO_2 \text{ (out)}}{CO_2 \text{ (in)}} \times 100 \quad (3)$$

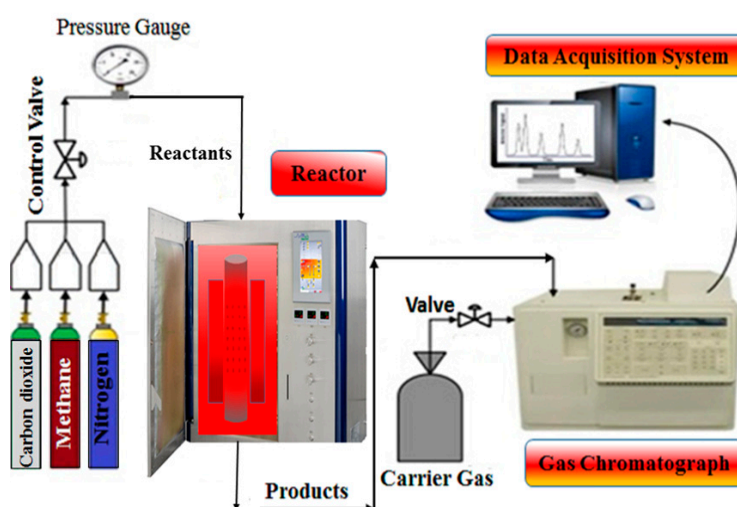


Figure 12. Schematic diagram of experimental setup for dry reforming of methane.

The same units and conditions stated in our previous paper [7] were used for the BET, TPD, TPR, XRD, TEM, and TGA analyses in the characterization of catalysts before/after reactions.

In the present work, blank runs were performed using similar operating conditions. The results obtained at 800 °C reaction temperature displayed nearly no conversion activity. In addition, using the same experimental conditions we did the blank test using the MCM-41 support alone without active metal of the catalyst. Again, the activity attained was negligible.

#### 4. Conclusions

The incipient wetness impregnation method was employed to form Ni/MCM-41 mesoporous catalysts. Syngas production via CO<sub>2</sub> DRM was investigated using the catalysts. The influence of different Ga loadings (0.0, 1.0, 1.5, 2.0, 2.5, and 3.0 wt %) on the catalytic performance was evaluated after testing and characterizing the catalysts. Ga doping positively affected the surface area. Moreover, the incorporation of Ga to the catalyst decreased the number of both strong and medium basic sites. Carbon deposition over the catalyst also decreased with the addition of Ga. A CH<sub>4</sub> conversion of 88.2% was achieved with 2% Ga loading, which also gave the highest stability with only a 1.58% activity loss. Ga as a promoter has a significant effect on the H<sub>2</sub>/CO ratio, as the ratio increased from 0.9 to unity with the addition of Ga.

**Author Contributions:** A.S.A.-F., A.H.F., A.A.I., and A.S.A.-A. performed all experiments and characterization tests as well as shared in the analysis of the data and share in the writing of the manuscript. Both J.K.A.-D. and A.E.A. wrote the paper and shared in data analysis. A.M.E.-T has performed XRD and TEM measurements and data analysis as well as sharing in writing the manuscript.

**Acknowledgments:** Sincere appreciation was sent to the Deanship of Scientific Research at King Saud University for financially supporting the research group project no. RG-1436-119. The authors also thank the Deanship of Scientific Research and RSSU at King Saud University for their technical support.

**Conflicts of Interest:** The investigators confess the absence of conflict of interest.

#### References

1. Tian, C.L.H.; Ciaisi, P.; Michalak, A.M.; Canadell, J.G.; Saikawa, E.; Huntzinger, D.N.; Gurney, K.R.; Sitch, S.; Zhang, B.; Yang, J.; et al. The terrestrial biosphere as a net source of greenhouse gases to the atmosphere. *Nature* **2015**, *531*, 225–228. [[CrossRef](#)] [[PubMed](#)]
2. Lunsford, J.H. Catalytic conversion of methane to more useful chemicals and fuels: A challenge for the 21st century. *Catal. Today* **2000**, *63*, 165–174. [[CrossRef](#)]
3. Omae, L. Aspects of carbon dioxide utilization. *Catal. Today* **2006**, *115*, 33–52. [[CrossRef](#)]
4. Liu, D.; Cheo, W.N.; Lau, R.; Borgna, A.; Yang, Y.J. MCM-41 supported nickel-based bimetallic catalysts with superior stability during carbon dioxide reforming of methane: Effect of strong metal-support interaction. *J. Catal.* **2009**, *266*, 380–390. [[CrossRef](#)]
5. Bradford, M.C.J.; Vannice, M.A. CO<sub>2</sub> reforming of methane. *Catal. Rev.* **1999**, *41*, 1–42. [[CrossRef](#)]
6. Li, D.L.Y.; Wang, G. Methane decomposition to CO<sub>x</sub>-free hydrogen and nano-carbon material on group 8-10 base metal catalysts: A review. *Catal. Today* **2011**, *162*, 1–48. [[CrossRef](#)]
7. Al-Fatesh, A.S.; Amin, A.; Ibrahim, A.A.; Khan, W.U.; Soliman, M.A.; AL-Otaibi, R.L.; Fakeeha, A.H. Effect of Ce and Co Addition to Fe/Al<sub>2</sub>O<sub>3</sub> for Catalytic Methane Decomposition. *Catalysts* **2016**, *6*, 40. [[CrossRef](#)]
8. Usman, M.M.; Wan Daud, W.M.A.; Abbas, H.F. Dry reforming of methane: Influence of process parameters—A review. *Renew. Sustain. Energy Rev.* **2015**, *45*, 710–744. [[CrossRef](#)]
9. Eltejaei, H.; Bozorgzadeh, J.T.H. R.; Omidkhah, M.R.; Rezaei, M.; Zanganeh, R.; Zamaniyan, A.; Ghalam, A.Z. Methane dry reforming on Ni/Ce<sub>0.75</sub>Zr<sub>0.25</sub>O<sub>2</sub>-MgAl<sub>2</sub>O<sub>4</sub> and Ni/Ce<sub>0.75</sub>Zr<sub>0.25</sub>O<sub>2</sub>-gamma-alumina: Effects of support composition and water addition. *Int. J. Hydrogen Energy* **2012**, *37*, 4107–4118. [[CrossRef](#)]
10. Wolfbeisser, O.S.A.; Bernardi, J.; Wittayakun, J.; Föttinger, K.; Rupprechter, G. Methane dry reforming over ceria-zirconia supported Ni catalysts. *Catal. Today* **2016**, *277*, 234–245. [[CrossRef](#)]
11. Rahemi, N.; Haghghi, M.; Babaluo, A.A.; Jafari, M.F.; Estifae, P. Synthesis and physicochemical characterizations of Ni/Al<sub>2</sub>O<sub>3</sub>-ZrO<sub>2</sub> nanocatalyst prepared via impregnation method and treated with non-thermal plasma for CO<sub>2</sub> reforming of CH<sub>4</sub>. *J. Ind. Eng. Chem.* **2013**, *19*, 1566–1576. [[CrossRef](#)]

12. Aghamohammadi, S.; Haghghi, M.; Karimipour, S. A comparative synthesis and physicochemical characterizations of Ni/Al<sub>2</sub>O<sub>3</sub>-MgO nanocatalyst via sequential impregnation and sol-gel methods used for CO<sub>2</sub> reforming of methane. *Nanosci. Nanotechnol.* **2013**, *13*, 4872–4882. [[CrossRef](#)]
13. Sener, T.D.C.; Dogu, G. Effects of synthesis conditions on the structure of Pd incorporated MCM-41 type mesoporous nanocomposite catalytic materials with high Pd/Si ratios. *Microporous Mesoporous Mater.* **2006**, *94*, 89–98. [[CrossRef](#)]
14. Amin, M.H.; Tardio, J.; Bhargava, S.K. A comparison study on carbon dioxide reforming of methane over Ni catalysts supported on mesoporous SBA-15, MCM-41, KIT-6 and gamma-Al<sub>2</sub>O<sub>3</sub>. In *Chemeca 2013: Challenging Tomorrow*; Engineers Australia: Brisbane, Australia, 2013; pp. 543–548.
15. Chen, X.W.C.; Zhang, L.; Zou, X.; Ding, W.; Lu, X. Synthesis of mesoporous Ni-La<sub>2</sub>O<sub>3</sub>/SiO<sub>2</sub> by poly(ethylene glycol)-assisted sol-gel route as highly efficient catalysts for dry reforming of methane with a H<sub>2</sub>/CO ratio of unity. *Catal. Commun.* **2017**, *94*, 38–41. [[CrossRef](#)]
16. Deshmane, V.G.; Abrokwah, R.Y.; Kuila, D. Synthesis of stable Cu-MCM-41 nanocatalysts for H<sub>2</sub> production with high selectivity via steam reforming of methanol. *Int. J. Hydrogen Energy* **2015**, *40*, 10439–10452. [[CrossRef](#)]
17. Abrokwah, R.Y.; Deshmane, V.G.; Kuila, D. Comparative performance of MMCM-41(M: Cu, Co, Ni, Pd, Zn and Sn) catalysts for steam reforming of methanol. *J. Mol. Catal. A Chem.* **2016**, *425*, 10–20. [[CrossRef](#)]
18. Damyanova, B.P.S.; Arishtirova, K.; Fierro, J.L.G.; Sener, C.; Dogu, T. MCM-41 supported PdNi catalysts for dry reforming of methane. *Appl. Catal. B* **2009**, *92*, 250–261. [[CrossRef](#)]
19. Liu, D.; Quek, X.Y.; Wah, H.H.A.; Zeng, G.; Li, Y.; Yang, Y. Carbon dioxide reforming of methane over nickel-grafted SBA-15 and MCM-41 catalysts. *Catal. Today* **2009**, *148*, 243–250. [[CrossRef](#)]
20. Liu, D.; Lau, R.; Borgna, A.; Yang, Y. Carbon dioxide reforming of methane to synthesis gas over Ni-MCM-41 catalysts. *Appl. Catal. A* **2009**, *358*, 110–118. [[CrossRef](#)]
21. Lovell, Y.J.E.; Scott, J.; Wang, F.; Suhardja, Y.; Chen, M.; Huang, J.; Amal, R. CO<sub>2</sub> reforming of methane over MCM-41-supported nickel catalysts: Altering support acidity by one-pot synthesis at room temperature. *Appl. Catal. A* **2014**, *473*, 51–58. [[CrossRef](#)]
22. Xu, L.; Song, H.; Chou, L. Carbon dioxide reforming of methane over ordered mesoporous NiO-MgO-Al<sub>2</sub>O<sub>3</sub> composite oxides. *Appl. Catal. B* **2011**, *108*, 177–190. [[CrossRef](#)]
23. Zhang, S.M.S.; Ishiguro, N.; Tada, M. Ceria-Doped Ni/SBA-16 Catalysts for Dry Reforming of Methane. *ACS Catal.* **2013**, *3*, 1855–1864. [[CrossRef](#)]
24. Arbag, S.Y.H.; Yasyerli, N.; Dogu, G. Activity and stability enhancement of Ni-MCM-41 catalysts by Rh incorporation for hydrogen from dry reforming of methane. *Int. J. Hydrogen Energy* **2010**, *35*, 2296–2304. [[CrossRef](#)]
25. Ambursa, M.M.; Sudarsanam, P.; Voon, L.H.; Hamid, S.B.; Bhargava, S.K. Bimetallic Cu-Ni catalysts supported on MCM-41 and Ti-MCM-41 porous materials for hydrodeoxygenation of lignin model compound into transportation fuels. *Fuel Process. Technol.* **2017**, *162*, 87–97. [[CrossRef](#)]
26. Liu, D.; Cheo, W.N.; Lim, Y.W.; Borgna, A.; Lau, R.; Yang, Y. A comparative study on catalyst deactivation of nickel and cobalt incorporated MCM-41 catalysts modified by platinum in methane reforming with carbon dioxide. *Catal. Today* **2010**, *154*, 229–236. [[CrossRef](#)]
27. Ochoa, J.V.; Malmusi, A.; Recchi, C.; Cavani, F. Understanding the Role of Gallium as a Promoter of Magnesium Silicate Catalysts for the Conversion of Ethanol into Butadiene. *ChemCatChem* **2017**, *9*, 2128–2135. [[CrossRef](#)]
28. Medina, J.C.; Figueroa, M.; Manrique, R.; Pereira, J.R.; Srinivasan, P.D.; Bravo-Suárez, J.J.; Medrano, V.G.; Jiménez, R.; Karelavic, A. Catalytic consequences of Ga promotion on Cu for CO<sub>2</sub> hydrogenation to methanol. *Catal. Sci. Technol.* **2017**, *7*, 3375–3387. [[CrossRef](#)]
29. Ruff, J.K. Friedel-Crafts and Related Reactions. Volume I: General Aspects. By George Olah. *Inorg. Chem.* **1964**, *3*, 1205–1206. [[CrossRef](#)]
30. Häfele, A.R.M.; Roppelt, D.; Emig, G. Hydroxylation of benzene with nitrous oxide on H-Ga-ZSM5 zeolite. *Appl. Catal. A* **1997**, *150*, 153–164. [[CrossRef](#)]
31. Ibrahim, A.A.; Fakeeha, A.H. Al-Fatesh, A.S. Enhancing hydrogen production by dry reforming process with strontium promoter. *Int. J. Hydrogen Energy* **2014**, *39*, 1680–1687. [[CrossRef](#)]
32. Nguyen, H.K.D.; Dang, T.H.; Nguyen, N.L.T.; Nguyen, H.T.; Dinh, N.T. Novel Ni-Ga alloy based catalyst for converting CO<sub>2</sub> to methanol. *Can. J. Chem. Eng.* **2018**, *96*, 832–837. [[CrossRef](#)]

33. Studt, I.S.F.; Abild-Pedersen, F.; Elkjær, C.F.; Hummelshøj, J.S.; Dahl, S.; Chorkendorff, S.I.; Nørskov, J.K. Discovery of a Ni-Ga catalyst for carbon dioxide reduction to methanol. *Nat. Chem.* **2014**, *6*, 320–324. [[CrossRef](#)] [[PubMed](#)]
34. Wang, X.Y.N.; Wang, Y.; Chu, W.; Liu, M. A comparison study on methane dry reforming with carbon dioxide over LaNiO<sub>3</sub> perovskite catalysts supported on mesoporous SBA-15, MCM-41 and silica carrier. *Catal. Today* **2013**, *212*, 98–107. [[CrossRef](#)]
35. Lin, S.; Yang, L.; Yang, X.; Zhou, R. Redox properties and metal–support interaction of Pd/Ce<sub>0.67</sub>Zr<sub>0.33</sub>O<sub>2</sub>–Al<sub>2</sub>O<sub>3</sub> catalyst for CO, HC and NO<sub>x</sub> elimination. *Appl. Surf. Sci.* **2014**, *305*, 642–649. [[CrossRef](#)]
36. Supamathanon, J.W.N.; Prayoonpokarach, S.; Supronowicz, W.; Rößner, F. Basic properties of potassium oxide supported on zeolite y studied by pyrrole-tpd and catalytic conversion of methylbutynol *Quim. Nova* **2012**, *35*, 1719–1723.
37. Tsoncheva, L.I.T.; Rosenholm, J.; Linden, M. Cobalt oxide species supported on SBA-15, KIT-5 and KIT-6 mesoporous silicas for ethyl acetate total oxidation. *Appl. Catal. B* **2009**, *89*, 365–374. [[CrossRef](#)]
38. Samadi-Maybodi, M.T.A.; Vahid, A.; Miranbeigi, A. In situ incorporation of nickel nanoparticles into the mesopores of MCM-41 by manipulation of solvent-solute interaction and its activity toward adsorptive desulfurization of gas oil. *J. Hazard. Mater.* **2011**, *192*, 1667–1674. [[CrossRef](#)] [[PubMed](#)]
39. Dai, B.W.B.; Zhu, M.; Kang, L.; Yu, F. Nickel catalysts supported on amino-functionalized MCM-41 for syngas methanation. *RSC Adv.* **2016**, *6*, 66957–66962. [[CrossRef](#)]
40. Hassan, H.B.; Abdel Rahim, M.A.; Khalil, M.W.; Mohammed, R.F. Ni Modified MCM-41 as a Catalyst for Direct Methanol Fuel Cells. *Int. J. Electrochem. Sci* **2014**, *9*, 760–777.
41. Michorczyk, J.O.P.; Kuśtrowski, P.; Chmielarz, L. Chromium oxide supported on MCM-41 as a highly active and selective catalyst for dehydrogenation of propane with CO<sub>2</sub>. *Appl. Catal. A* **2008**, *349*, 62–69. [[CrossRef](#)]
42. Al-Fatish, A.S.A.; Ibrahim, A.A.; Fakeeha, A.H.; Soliman, M.A.; Siddiqui, M.R.H.; Abasaeed, A.E. Coke formation during CO<sub>2</sub> reforming of CH<sub>4</sub> over alumina-supported nickel catalysts. *Appl. Catal. A Gen.* **2009**, *364*, 150–155.



© 2018 by the authors. Licensee MDPI, Basel, Switzerland. This article is an open access article distributed under the terms and conditions of the Creative Commons Attribution (CC BY) license (<http://creativecommons.org/licenses/by/4.0/>).